

Article

# Fast Single-Parameter Energy Function Thresholding for Image Segmentation Based on Region Information

Rong Lan, Danlin Feng <sup>\*</sup>, Feng Zhao, Jiulun Fan and Haiyan YuSchool of Communications and Information Engineering & School of Artificial Intelligence,  
Xi'an University of Posts and Telecommunications, Xi'an 710121, China

\* Correspondence: fengfengddl@163.com

**Abstract:** To solve the problems of image threshold segmentation based on weak continuous constraint theory, the running time is long, and the two parameters need to be selected manually, and therefore a fast single-parameter energy function thresholding for image segmentation based on region information (FSEFTISRI) is proposed in this paper. The proposed FSEFTISRI algorithm uses simple linear iterative clustering (SLIC) technology to pre-block the image, extract the image super-pixels, and then map the image super-pixels to the interval type-2 fuzzy set (IT2FS), so as to construct the single-parameter energy function to search the optimal threshold, and adaptively select the penalty parameters in the energy function through the class uncertainty theory. On a non-destructive testing (NDT) database and Berkeley segmentation datasets and benchmarks (BSDS), the proposed FSEFTISRI is compared with five related algorithms. The average misclassification error (ME) of the proposed FSEFTISRI algorithm on NDT and BSDS are 0.0466 and 0.0039, respectively. The results show that the proposed FSEFTISRI has acquired more satisfactory results in visual effect and evaluation index, and the running time of the proposed FSEFTISRI algorithm is shorter, which shows the effectiveness of the proposed FSEFTISRI.

**Keywords:** class uncertainty theory; energy function; interval type-2 fuzzy set; super-pixel; threshold segmentation

MSC: 68T50



**Citation:** Lan, R.; Feng, D.; Zhao, F.; Fan, J.; Yu, H. Fast Single-Parameter Energy Function Thresholding for Image Segmentation Based on Region Information. *Mathematics* **2023**, *11*, 1059. <https://doi.org/10.3390/math11041059>

Academic Editor: Jakub Nalepa

Received: 14 January 2023

Revised: 7 February 2023

Accepted: 18 February 2023

Published: 20 February 2023



**Copyright:** © 2023 by the authors. Licensee MDPI, Basel, Switzerland. This article is an open access article distributed under the terms and conditions of the Creative Commons Attribution (CC BY) license (<https://creativecommons.org/licenses/by/4.0/>).

## 1. Introduction

Image segmentation refers to the procedure of dividing an image into some sub-regions according to the gray level, texture and other information of the image. It is one of the primary missions of image processing. Thresholding segmentation is widely used because of its clear physical meaning, obvious effect, easy implementation, and good real-time performance [1,2].

The uncertainty in an image brings challenges to the threshold segmentation technology. Fuzzy set theory, used by many image segmentation algorithms [3,4], is a powerful tool to process uncertain information. Since the membership function of a type-2 fuzzy set is fuzzy and has a stronger ability to deal with uncertain information, it has attracted extensive attention [5,6]. Furthermore, in order to solve the problem of poor segmentation results caused by the fuzziness and uncertainty of the image itself, many scholars have made attempts. SaHa et al. [7] provided a classical energy minimization algorithm based on class uncertainty and regional uniformity which can better deal with the fuzzy boundary in images. However, because of the global threshold, this algorithm has a poor segmentation effect on images with more noise or inhomogeneous gray distribution. Wang et al. [8] suggested a robust optimal thresholding algorithm based on local intensity mapping and class uncertainty theory, which has satisfactory segmentation results and robustness for fuzzy and noisy images. Zhou et al. [9] explored a local threshold segmentation algorithm

based on multi-scale region and class uncertainty theory (MRCUT). The MRCUT algorithm can effectively overcome the interference of noise, the uneven distribution of the local gray scale and fuzzy boundary, but the multi-layer block iterative optimization strategy leads to high computational complexity. Liang et al. [10] discussed a threshold segmentation algorithm combining class uncertainty and shape dissimilarity and applied it to data cleaning. Soumyadip et al. [11–13] first applied the weak continuity constraint theory which was used to vision reconstruction in an early stage to image segmentation to deal with the uncertainty in threshold segmentation, a threshold segmentation algorithm combining fuzzy set, and weak continuity theory was proposed and then improved. Following [12], an IT2FS and theory of weak continuity constraint (IT2FSWCC) for accurate multiclass image segmentation was presented which can better locate the segmentation boundary and reduce the uncertainty in the procedure of image segmentation. However, due to the influence of neighborhood scale calculation, the IT2FSWCC algorithm takes a long time. Following [13], an accurate multi-class image segmentation using a neutrosophic set and weak continuity constraints (NSWCC) was discussed, which maps an image to a neutrosophic set for segmentation. Although the operation time is reduced, this improvement comes at the cost of segmentation accuracy.

Super-pixel segmentation technology can group pixels with adjacent positions and similar pixel characteristics to form a limited number of super-pixels. As a preprocessing step of the image threshold algorithm, super-pixel segmentation technology can effectively reduce the computational complexity of the algorithm. Achanta et al. [14] used SLIC to obtain image super-pixels, which can better fit the image boundary and in a faster manner; Lei et al. [15] proposed the algorithm of multi-scale morphological gradient reconstruction to generate the super-pixel image with a clear contour. The algorithm provides an adaptive and irregular local spatial neighborhood. Di et al. [16] improved SLIC through the method of multi-level layering to adaptively select the number of super-pixels. He et al. [17] improved the square neighborhood of SLIC to a circular neighborhood, and selected different transformation parameters by means of the conditional iterative algorithm, which made the algorithm more suitable for microscopic cell images. Zhang et al. [18] adopted a noniterative framework to generate super-pixels quickly and accurately by processing all pixels at once.

Recently, many segmentation algorithms have been found to reduce the labor costs by automatically segmenting the specified targets in images, such as aircraft fuselage and lesions, etc. In order to segment images more accurately, the IT2FSWCC algorithm [12] describes the uncertain information in the image based on IT2FS and weak continuous constraint theory, and constructs the energy function for image segmentation. When mapping an image to IT2FS, it is necessary to calculate the corresponding fuzzy set for each selected threshold. The energy function based on weak continuous constraint theory needs to calculate the  $7 \times 7$  or  $13 \times 13$  neighborhood information of pixels. The IT2FSWCC algorithm has a very long running time due to the above two aspects. At the same time, the manual selection of spatial parameters  $\lambda$  and penalty parameters  $\alpha$  according to the experiment is another aspect of the IT2FSWCC algorithm that needs to be improved. The spatial parameters  $\lambda$  control the scale of the neighborhood, which needs to be selected manually through a large number of experiments and then combined with the spectral flatness measure of the image; the penalty parameters should be selected according to extensive experiments and the contrast between the target and the background.

To solve the problems that the IT2FSWCC algorithm runs for a long time and parameters cannot be selected adaptively, this paper proposes a fast single-parameter energy function thresholding for image segmentation based on region information. The IT2FS is used as a tool to process the uncertainty, and the energy function is improved as the objective function to search for the best threshold according the super-pixel technology. The new objective function includes global information and local information, which is improved based on SLIC, so that the uncertainty of the image can be described and the accuracy of the segmentation results can be improved. SLIC is used to convert the pixel

information of an image into regional information so as to improve the efficiency. Besides, penalty parameters are selected adaptively according to class uncertainty to reduce the impact of manual parameter selection on algorithm performance. The main innovations are as follows:

- (1) This paper pre-blocks the input image by SLIC to acquire the super-pixels of the image, which effectively reduces the number of pixels to be calculated and reduces the number of mapping times of an image to IT2FS and improves the efficiency of the algorithm;
- (2) The idea of an extended neighborhood is introduced to construct the energy function improved by the super-pixel, which can expand the neighborhood range of super-pixels to the whole homogeneous region and extract the irregular region spatial features of super-pixels without considering the parameter selection of the traditional neighborhood;
- (3) Another innovation of this paper lies in the adaptive selection of penalty parameters by using class-uncertainty theory, and the reduction in the subjective impact of manual selection parameters on segmentation performance to improve the adaptability of the algorithm.

The rest of this paper proceeds as follows: Section 2 introduces basic theories, Section 3 shows the proposed FSEFTISRI algorithm, Section 4 reveals experimental results and analysis, and Section 5 draws conclusions.

## 2. Basic Theories

In this paper, IT2FS theory [19] is used to describe image information, and weak continuous constraint theory [12] is used to construct the energy function. This section mainly introduces the basic concepts of IT2FS and energy function.

### 2.1. Interval Type-2 Fuzzy Set

Type-2 fuzzy sets  $\tilde{A}$  are generally defined by type-2 fuzzy membership functions  $\mu_{\tilde{A}}(x, u)$ ,

$$\tilde{A} = \{((x, u), \mu_{\tilde{A}}(x, u)) | \forall x \in X, \forall u \in J_x \subseteq [0, 1]\} \tag{1}$$

where,  $0 \leq \mu_{\tilde{A}}(x, u) \leq 1$ ,  $\tilde{A}$  can also be expressed as follows:

$$\tilde{A} = \int_{x \in X} \int_{u \in J_x} \mu_{\tilde{A}}(x, u) / (x, u), J_x \subseteq [0, 1] \tag{2}$$

in which  $J_x$  is the primary membership function,  $\mu_{\tilde{A}}(x, u)$  represents the sub-membership function, and for discrete sets,  $\int$  can be replaced by  $\Sigma$ .

When all  $\mu_{\tilde{A}}(x, u) = 1$  in Equation (2),  $\tilde{A}$  represents IT2FS.

### 2.2. Energy Function Based on Weak Continuity Constraints

To construct the energy function based on the weak continuous constraint theory, it is essential to count the neighborhood information of all pixels in an image [12] so as to consider the local information of the image when dealing with the uncertain information. According to weak string theory under weak continuous constraints, when a group of data violates the constraints, it must pay a price, that is, when the continuous constraints are broken, the penalty term plays a role as a price, which is helpful in locating the discontinuous points locally.

As shown in Ref. [12], the weak string theory under the weak continuity constraint is applied to image segmentation. On the basis of this theory, the string attempts to remain stable at the lowest energy. In the segmentation process, each pixel is interpolated into the target or background through their centroids  $v(R_i), i = 1, 2$ , the segmentation boundary points lead to string breaking and the discontinuities are localized because of the violation of weak

continuity constraints. Accurate segmentation results are attained by minimizing the energy function. The calculation formula of the energy function is shown in Equation (3)

$$E = D + S + P \tag{3}$$

where,

$$D = \sum_{i=1}^2 \sum_{x \in R_i} (x - v(R_i))^2 \tag{4}$$

$$S = \lambda^2 \sum_{i=1}^2 \sum_{x \in R_i} \sum_{y \in N_x} (\mu(x) - \mu(y))^2 (1 - b(x)) \tag{5}$$

$$P = \alpha \sum_{i=1}^2 \sum_{x \in R_i} b(x) \tag{6}$$

here,  $\mu(x)$  denotes the membership value of pixel  $x$ , and  $N_x$  represents the adjacent pixels in a local window of size  $\lambda \times \lambda$ .  $v(R_i)$  is the IT2FS center of gravity of the target or background  $R_i$ . Boundary point  $b(x) = 1$ , non-boundary point  $b(x) = 0$ .

### 3. The Proposed FSEFTISRI Algorithm

This paper mainly discusses the image segmentation based on energy function. The aim is to overcome the shortcomings of the IT2FSWCC algorithm, and the fast single-parameter energy function thresholding for image segmentation based on region information is proposed.

The proposed FSEFTISRI algorithm is based on IT2FS theory. First, the image is segmented by SLIC to obtain the image super-pixel. Based on the super-pixel, an improved energy function combining region information of the image is constructed according to the weak continuous constraint theory. At the same time, the neighborhood of the super-pixel is extended to the whole homogeneous area, and the idea of an extended neighborhood is introduced for the image super-pixel. Thus, the selection of spatial parameters  $\lambda$  in the original energy function does not need to be considered. Furthermore, the class-uncertainty is used to select the penalty parameters  $\alpha$  adaptively. Finally, the improved energy function is minimized to search the optimal threshold. The flow of each part of the proposed FSEFTISRI algorithm is drawn in Figure 1.

#### 3.1. Mapping Image to IT2FS

The proposed FSEFTISRI uses the concept of IT2FS as a tool to construct a mathematical model of the image to describe the uncertain and inaccurate information in the image. Therefore, the image is mapped to IT2FS first, and the type-1 membership function of the image target and background is given by the following equation:

$$\mu(k) = \begin{cases} 1 - (\frac{k}{t})^{\varepsilon_1}, & k \leq t \\ 1 - (\frac{L-k}{L-t})^{\varepsilon_2}, & k > t \end{cases} \tag{7}$$

where,  $\varepsilon_1, \varepsilon_2 > 0$ ,  $k$  is super-pixel gray value, and  $t$  is the threshold value.

The interval type-2 membership function is generated through the type-1 fuzzy membership function shown in Equation (7). The calculation expressions of the upper and lower membership functions  $\bar{\mu}$  and  $\underline{\mu}$  are shown in Equation (8):

$$\begin{aligned} \bar{\mu}(k) &= \mu(k)^{\frac{1}{\beta}} \\ \underline{\mu}(k) &= \mu(k)^\beta \end{aligned} \tag{8}$$

where,  $\beta \in (1, \infty)$ . Equation (7) shows that a different threshold,  $t$  will produce a different fuzzy set, resulting in a different IT2FS.

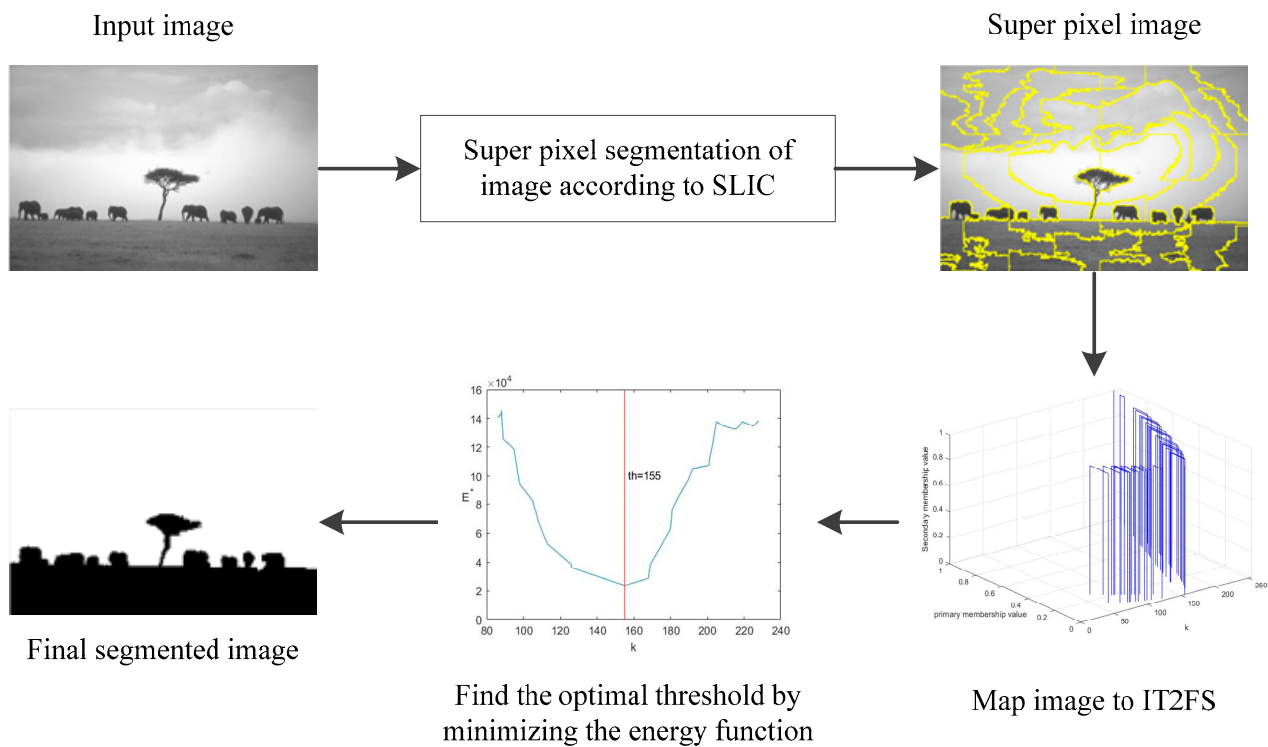


Figure 1. Flow chart of the proposed FSEFTISRI algorithm.

### 3.2. Single-Parameter Energy Function Combining with Region Information

The SLIC algorithm pre-segments the image into a fixed number of super-pixels based on the color feature  $[l_{si}, a_{si}, b_{si}]$  and position feature  $[x_{si}, y_{si}]$  of the pixel [14], which changes the image from pixel level to region level. The proposed FSEFTISRI mainly discusses the gray image, so only the brightness similarity and spatial adjacency in SLIC are used to calculate the distance  $d(si, sj)$  between the candidate pixel  $sj$  and the cluster center  $si$ , which is defined as:

$$d(si, sj) = \sqrt{d_l^2(si, sj) + \left(\frac{m}{Space}\right)^2 d_{xy}^2(si, sj)} \tag{9}$$

$$d_{xy}(si, sj) = \sqrt{(x_{si} - x_{sj})^2 + (y_{si} - y_{sj})^2} \tag{10}$$

$$d_l(si, sj) = \sqrt{(l_{si} - l_{sj})^2} \tag{11}$$

where,  $d_{xy}$  represents the spatial position distance and  $d_l$  represents the brightness distance.  $Space = \sqrt{N/K}$  represents the distance between neighboring seed points,  $N$  is the number of image pixels,  $m$  represents the weight coefficient, usually,  $m \in [1, 40]$ .

The pixels of the image are transformed into super-pixels through SLIC. Figure 2a is an image #253036 from BSDS [20]. Figure 2b is obtained after super-pixel segmentation ( $K = 30$ ). The yellow curve is the boundary of super-pixels.

It should be explained that  $m = 10$  in the common SLIC technology will result in more regular super-pixels, because the larger the  $m$  is, the greater the proportion of spatial distance  $d_{xy}$  in  $d$  is, and the greater the impact of spatial position on the generation of super-pixels, the more regular super-pixels will be generated. However, experiments show that  $m$  in the proposed FSEFTISRI should be 1 so that each super-pixel is as irregular as possible, because the super-pixels generated by the proposed FSEFTISRI are bigger than those generated by the common SLIC. If the super-pixel is a regular  $n$ -polygon, it cannot fit the target boundary accurately.

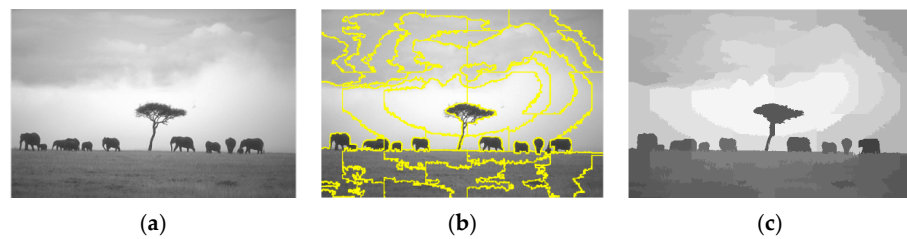


**Figure 2.** Super-pixel segmentation diagram of image #253036 from BSDS ( $K = 30$ ): (a) Original image, (b) Super-pixel boundary, (c) Super-pixel averaging image.

The super-pixel of the image is composed of multiple pixels, so it is necessary to select statistics to describe the brightness information of the super-pixel block as its gray feature. Therefore, the gray mean of each super-pixel is taken. When calculating the energy function, we take the mean as the gray value of the super-pixel, as shown in Figure 2c. In other words, the gray mean of all pixels in a super-pixel is the value of the super-pixel.

In Equation (5), the spatial feature  $S$  denotes the change of membership value in the neighborhood with scale  $\lambda$ . Because the IT2FSWCC algorithm calculates the stretching energy based on the square neighborhood of a single pixel, that is, the change of membership value in the neighborhood with scale  $\lambda$ , the performance of the IT2FSWCC algorithm is limited and affected by the neighborhood scale parameter  $\lambda$ . The proposed FSEFTISRI algorithm then uses the super-pixel strategy to pre-block the image. Since the super-pixel has an irregular shape, it is not suitable to use the traditional neighborhood to represent the stretching energy.

Therefore, the pixel neighborhood is generalized, and the idea of an extended neighborhood is introduced for the image super-pixel in this paper. Based on the idea of extended neighborhood, the stretching energy is obtained by counting the sum of changes in membership values between all pairs of super-pixels. This strategy can not only extract the spatial features of irregular super-pixels, but also does not need to consider the selection of traditional neighborhood parameter  $\lambda$ . Since the number of super-pixels is far fewer than the number of image pixels, the computation of the proposed FSEFTISRI can be effectively reduced. In the proposed FSEFTISRI algorithm, the calculation formula of the improved spatial feature term  $S^*$  is as follows:

$$S^* = \sum_{i=1}^2 (N_{R_i} \sum_{k \in R_i} \sum_{\substack{k' \in R_i \\ k' \neq k}} (\mu(k) - \mu(k'))^2) \tag{12}$$

where,  $N_{R_i}$  represents the number of super-pixels in the target or background  $R_i$ ,  $\mu(k)$  and  $\mu(k')$  denotes the membership values of two super-pixels  $k$  and  $k'$  belonging to the same category, respectively.

Using the space feature term in Equation (12), a new energy function constructed as the objective function of the proposed FSEFTISRI algorithm and the specific formula is shown in Equation (13):

$$E^* = D^* + S^* + P^* \tag{13}$$

here, the distance term  $D^*$  and penalty term  $P^*$  are as follows:

$$D^* = \sum_{i=1}^2 \sum_{k \in R_i} (k - v(R_i))^2 \tag{14}$$

$$P^* = \alpha \sum_{i=1}^2 \sum_{k \in R_i} b(k^x) \tag{15}$$

where, center of gravity  $v(R_i)$  is calculated as follows:

$$v(R_i) = \frac{\sum_{k \in R_i} \mu(k) \cdot k}{\sum_{k \in R_i} \mu(k)} \tag{16}$$

here, the IT2FS needs to be reduced:  $\mu(k) = \frac{\bar{\mu}(k) + \mu(k)}{2}$ ,  $k$  represents gray value of super-pixel,  $b(k^x)$  denotes a Boolean value, which is 1 at the boundary point and 0 at the non-boundary point. Given a set of boundary pixels  $(x, x')$  satisfying  $\{(x, x') | (x, x') \text{ are adjacent, } x \leq t \& x' > t \text{ or } x > t \& x' \leq t\}$ .

**Remark 1.** A super-pixel is a collection of multiple pixels. When calculating the Boolean value, if the super-pixel is judged as a boundary super-pixel, only the Boolean values of pixels on the boundary of a super-pixel is set to 1, and the Boolean values of other pixels are set to 0.

Figure 3 shows the Boolean value of image #253036 (the original image ref. Figure 2a) under the optimal threshold, that is, the Boolean matrix of the image.

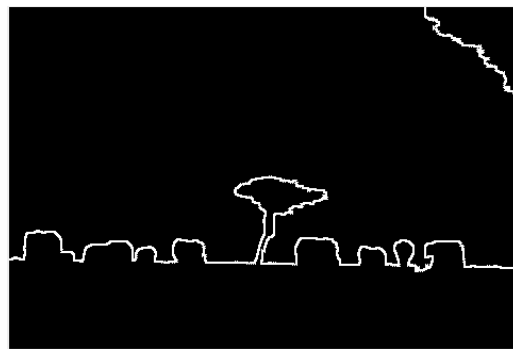


**Figure 3.** Boolean matrix of image #253036 from BSDS under optimal threshold.

### 3.3. Adaptive Selection of Uncertain Parameters $\alpha$

During the process of image segmentation, penalty term  $P^*$  is related to the location of discontinuities between target and background. In fact, both  $S^*$  and  $P^*$  in Equation (13) represent the spatial features of the image, and  $P^*$  can also be called the penalty term. As mentioned above, the super-pixel should be punished when it violates the weak continuity constraint, and the penalty term  $P^*$  in the energy function can reflect the cost it should pay.

In the proposed FSEFTISRI algorithm, the value of penalty parameter  $\alpha$  has a great impact on the penalty term  $P^*$ . If the value of  $\alpha$  is inappropriate, the algorithm may detect false inter class discontinuities. If the contrast between target and background is high,  $\alpha$  should be small. For this case, the value of energy function  $E^*$  decreases accordingly, which helps to minimize the energy function and obtain the optimal threshold. Otherwise,  $\alpha$  should be appropriately increased to avoid the detection of false discontinuities through increasing the value of energy  $E^*$ .

The theory of class uncertainty is based on the probability distribution of gray levels of the target or background in an image as prior knowledge to determine the uncertainty of image pixels belonging to the target or background under different thresholds. When the selected threshold is close to the optimal threshold, the class uncertainty of the image under this threshold is small. Figure 4 shows the class uncertainty of the image #253036 from BSDS [20] (shown in Figure 2a) under different super-pixel gray values. When the optimal threshold ( $th^* = 155$ ) is selected, the class uncertainty value of the image is the smallest.

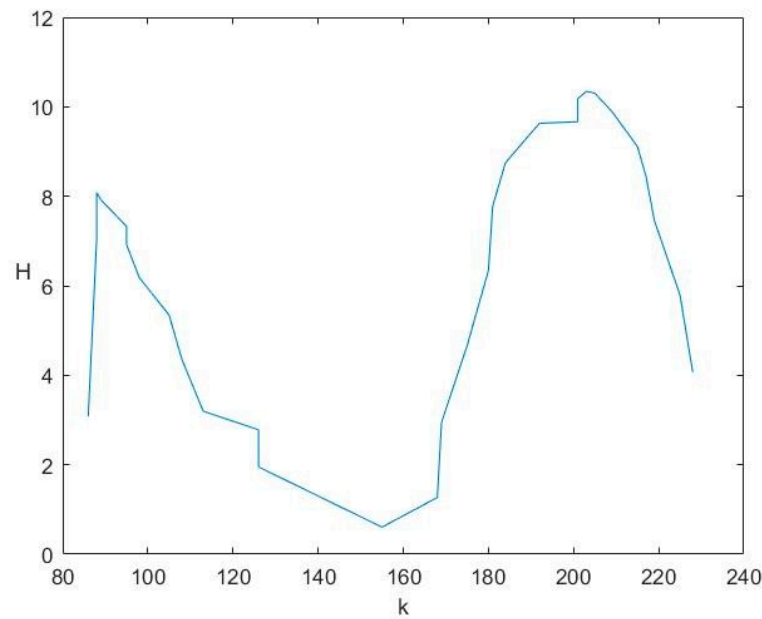


Figure 4. Variation curve of H value of image #253036 from BSDS with gray value.

The proposed FSEFTISRI selects parameter  $\alpha$  adaptively by calculating the class uncertainty of the image. When the selected threshold is closer to the optimal threshold, the class uncertainty value calculated by the threshold is smaller, so that the value of penalty term  $P^*$  is smaller and the value of energy function  $E^*$  is smaller; When the selected threshold is far from the optimal threshold, the class uncertainty value of the image is large, so the penalty term  $P^*$  value is large, which greatly affects the value of the energy function  $E^*$ , which has a positive impact on minimizing the energy function to calculate the optimal threshold.

The following is the class uncertainty  $H_t(k)$  with a super-pixel value of  $k$  at threshold  $t$  defined by Shannon entropy:

$$H_t(k) = -\frac{\theta(t)p_{1,t}(k)}{p_t(k)} \log \frac{\theta(t)p_{1,t}(k)}{p_t(k)} - \frac{(1-\theta(t))p_{2,t}(k)}{p_t(k)} \log \frac{(1-\theta(t))p_{2,t}(k)}{p_t(k)} \quad (17)$$

where,  $\theta(t)$  is the prior probability that the super-pixel belongs to the target at the threshold  $t$ ,  $p_{1,t}(k)$  and  $p_{2,t}(k)$  are the probability density functions of gray  $k$  belonging to the target and background pixels at the threshold  $t$  respectively. The calculations are as follows:

$$p_{1,t}(k) = \frac{1}{\sqrt{2\pi}\sigma_1(t)} e^{-\frac{(k-m_1(t))^2}{2\sigma_1(t)^2}} \quad (18)$$

$$p_{2,t}(k) = \frac{1}{\sqrt{2\pi}\sigma_2(t)} e^{-\frac{(k-m_2(t))^2}{2\sigma_2(t)^2}} \quad (19)$$

where,  $\sigma_1(t)$  and  $\sigma_2(t)$  represent the standard deviation of the super-pixel intensity belonging to the target and background,  $m_1(t)$  and  $m_2(t)$  are the average values of the super-pixel intensities belonging to the target and the background respectively.

According to Equations (18) and (19), the calculation formula of  $p_t(k)$  is constructed as follows:

$$p_t(k) = \theta(t)p_{1,t}(k) + (1-\theta(t))p_{2,t}(k) \quad (20)$$

In summary, the penalty parameter  $\alpha$  in Equation (15) can be calculated as follows:

$$\alpha = \sum_{k \in R} H_t(k) \quad (21)$$

where  $R$  represents the whole image.

### 3.4. The Steps of the Proposed FSEFTISRI Algorithm

To overcome the shortcomings of the IT2FSWCC algorithm, which has a long running time and cannot adaptively select parameters, the fast single-parameter energy function thresholding for image segmentation based on region information is proposed. The proposed FSEFTISRI algorithm uses SLIC to segment the super-pixel of the image, and improves the calculation of pixel information to the calculation of super-pixel information of the image, which effectively improves the operation efficiency of the algorithm. At the same time, the  $\lambda \times \lambda$  neighborhood of the image pixel is extended to all homogeneous regions of the super-pixel. According to the class uncertainty of the image, the penalty parameters are selected adaptively to improve the adaptability of the algorithm. The proposed FSEFTISRI algorithm is shown in Algorithm 1.

---

**Algorithm 1.** The proposed FSEFTISRI algorithm.

---

**FSEFTISRI:** A fast single-parameter energy function thresholding for image segmentation based on region information

Input: The gray level image  $img$ .

Output: Optimal threshold  $th^*$ , image segmented by optimal threshold.

**Step 1:** Generate  $K$  super-pixels by SLIC.

**Step 2:** Calculate the gray mean  $k$  of each super-pixel and sort it from small to large.

**Step 3:** For each super-pixel value  $k$ :

- (a) Transform super-pixel  $k_j$  to T1FS according to Equation (7)
- (b) Calculate the IT2FS according to T1FS through Equation (8)
- (c) Calculate  $v(R_1)$  and  $v(R_2)$  for sets  $[k_1, k_j]$  and  $[k_j, k_K]$  by Equation (16), then, the distance term  $D^*$  is calculated according to Equation (14)
- (d) Compute the spatial feature term  $S^*$  and penalty term  $P^*$  by Equation (12) and Equation (21) respectively
- (e) Compute  $E^* = D^* + S^* + P^*$

**Step 4:** Find  $k_j$  for which  $E^*$  is minimum is the optimal threshold  $th^*$ .

**Step 5:** Segment the image by the optimal threshold  $th^*$ .

---

### 3.5. Computational Complexity

To objectively analyze the operating efficiency of the proposed FSEFTISRI, the time complexity of the proposed FSEFTISRI is shown in this section. Assume that an image has  $N$  pixels and is divided into  $K$  super-pixels, then the computational complexity of the proposed FSEFTISRI algorithm is  $O(K^2 + N)$ .

Accordingly, the computational complexity of IT2FSWCC algorithm is  $O(N^2)$ .

Since the number of pixels  $K$  is far fewer than the number of pixels  $N$ , the computational complexity of the proposed FSEFTISRI algorithm is much smaller than that of the IT2FSWCC algorithm.

The proposed FSEFTISRI algorithm improves the IT2FSWCC algorithm through SLIC technology, which seems to use a more complex process, but the addition of SLIC generates super-pixels, which greatly reduces the calculation times of the objective function and its neighborhood information, and also reduces the mapping times of the image to IT2FS, so the efficiency of the proposed FSEFTISRI algorithm is improved.

## 4. Experimental Results and Analysis

This section introduces the experimental results and analysis. The experiment was performed on a PC with AMD Ryzen 7 5800H with Radeon Graphics (3.20 GHz) CPU and 16 GB of memory on a Windows 10 (64-bit) operating system. The software specification is MATLAB R2018a.

#### 4.1. Comparison Algorithm and Quantitative Evaluation Index

The proposed FSEFTISRI algorithm is compared with five related algorithms, such as Otus [21], a local threshold algorithm based on class uncertainty such as MRCUT [9], algorithms based on weak continuous constraint theory such as IT2FSWCC [12], and NSWCC [13], an algorithm based on energy function minimization technology such as EITMIS [22], to verify the performance of the proposed FSEFTISRI in segmentation visual effect and quantization index.

To objectively evaluate the segmentation performance of each algorithm, ME [23], feature similarity (FSIM) [24], peak signal-to-noise ratio (PSNR) [25] and structural similarity (SSIM) [26] are used as evaluation indexes to quantitatively analyze the experimental results.

ME is used to measure the ratio of misclassified pixels in all pixels. The smaller the value is, the fewer misclassified pixels are and the more accurate the segmentation result is.  $ME \in [0, 1]$ .

FSIM is a measure of similarity between two images. The range of FSIM is  $[0, 1]$ . For the satisfactory segmented images, a higher FSIM is required.

PSNR is an objective standard to measure image distortion, which can be computed by mean square error, and its unit is dB. The higher the PSNR is, the lower the distortion it represents. The minimum value of PSNR is 0, and there is no fixed upper limit.

SSIM is an index to evaluate the similarity between two images.  $SSIM \in [0, 1]$ . Higher SSIM means better image segmentation.

#### 4.2. Experimental Results and Analysis

In order to test the performance of the proposed FSEFTISRI algorithm, simulation experiments were conducted on two image databases: the NDT database [27] and the BSDS [20]. The visual segmentation effects of NDT and BSDS are revealed in Sections 4.2.1 and 4.2.2, respectively. In order to verify the stability of the proposed algorithm, Section 4.2.3 introduces the mean and variance of the evaluation indicators of 50 images from BSDS and 10 NDT images. In addition, the line chart of the evaluation indicators of 50 images from BSDS is also described in Section 4.2.3. The comparison experiment of the operation efficiency of the six algorithms is shown in Section 4.2.4.

When the IT2FS of the image is established,  $\varepsilon_1 = 0.25$ ,  $\varepsilon_2 = 0.75$ ,  $\beta = 1.25$ . In addition, this paper sets the number of pixels  $K = 100$  for NDT database and  $K = 30$  for BSDS.

##### 4.2.1. Analysis of Experimental Results of NDT Images

NDT image segmentation can be used for industrial fault detection. The NDT dataset includes 25 images and their ground images, including eddy current for thermal, printed circuit board images, light microscope, and ultrasonic, etc. NDT images are often very fuzzy, so it is very difficult to segment defective parts from the image. In this section, the proposed FSEFTISRI and comparison algorithms are applied to NDT images with a high gray scale and spatial ambiguity. The visual effect of image segmentation is shown in Figures 5–10.

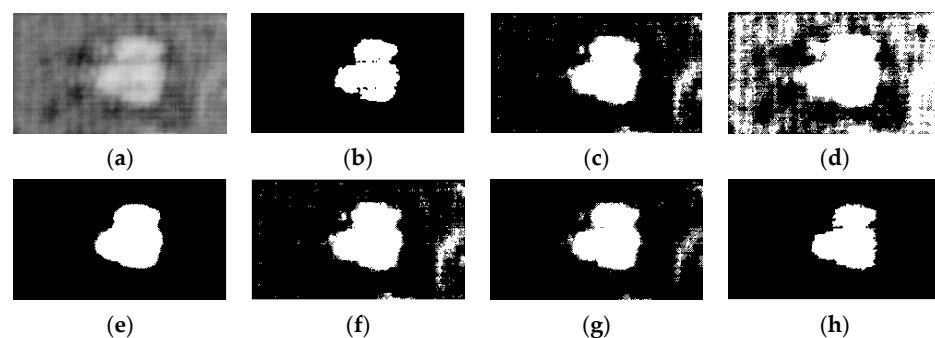


**Figure 5.** Image1 and its segmentation results: (a) #image1, (b) ground-truth, (c) Otus, (d) MRCUT, (e) EITMIS, (f) NSWCC, (g) IT2FSWCC, (h) FSEFTISRI.

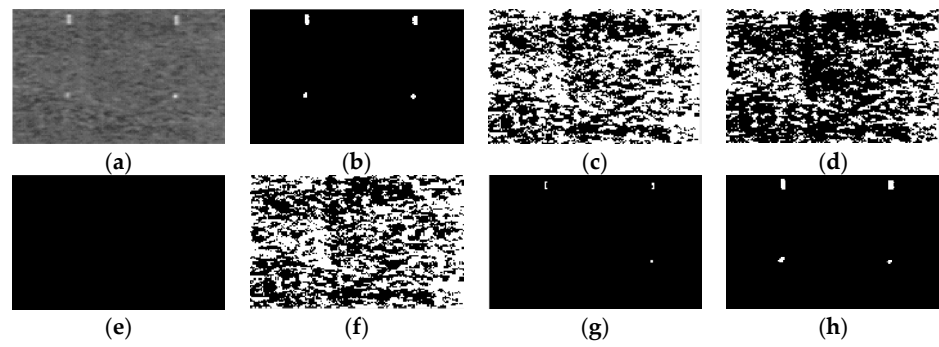


**Figure 6.** Image2 and its segmentation results: (a) #image2, (b) ground-truth, (c) Otus, (d) MRCUT, (e) EITMIS, (f) NSWCC, (g) IT2FSWCC, (h) FSEFTISRI.

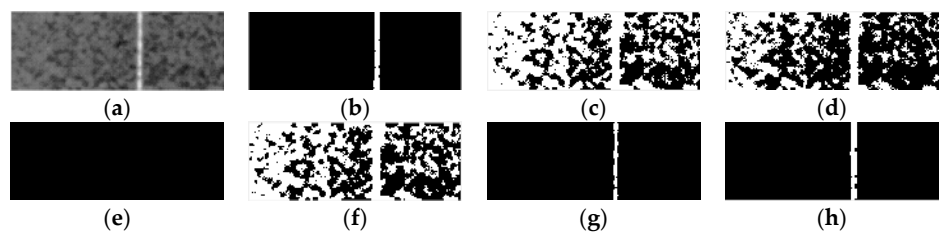


**Figure 7.** Image3 and its segmentation results: (a) #image3, (b) ground-truth, (c) Otus, (d) MRCUT, (e) EITMIS, (f) NSWCC, (g) IT2FSWCC, (h) FSEFTISRI.

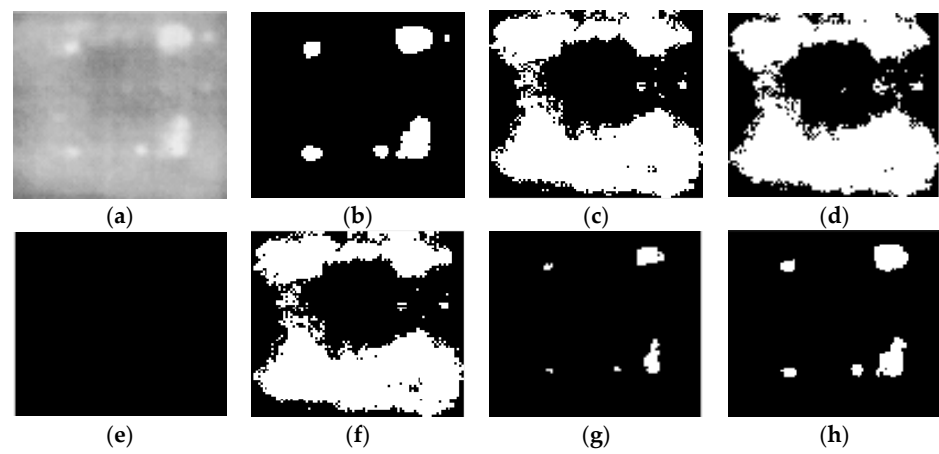


**Figure 8.** Image6 and its segmentation results: (a) #image6, (b) ground-truth, (c) Otus, (d) MRCUT, (e) EITMIS, (f) NSWCC, (g) IT2FSWCC, (h) FSEFTISRI.



**Figure 9.** Image13 and its segmentation results: (a) #image13, (b) ground-truth, (c) Otus, (d) MRCUT, (e) EITMIS, (f) NSWCC, (g) IT2FSWCC, (h) FSEFTISRI.



**Figure 10.** Image22 and its segmentation results: (a) #image22, (b) ground-truth, (c) Otus, (d) MRCUT, (e) EITMIS, (f) NSWCC, (g) IT2FSWCC, (h) FSEFTISRI.

From Figures 5–10, the proposed FSEFTISRI has satisfactory segmentation results on NDT images; the images after the segmentation of the proposed FSEFTISRI algorithm are closest to the ground-truth. In particular, as shown in Figures 6 and 7, both the IT2FSWCC algorithm and the proposed FSEFTISRI algorithm can obtain effective segmentation. In Figure 6, the proposed FSEFTISRI can completely segment four targets, while the segmentation result of IT2FSWCC misses a target: the white point in the lower left corner. In Figure 7, the proposed FSEFTISRI can completely segment the strip target and background, while the strip target of the IT2FSWCC algorithm is thinner than the ground-truth.

In Figure 10, the targets segmented by the MRCUT and IT2FSWCC algorithms are larger and smaller than the ground-truth, respectively, as the segmentation results are not ideal. At the same time, the segmentation results of Otus, NSWCC and the proposed FSEFTISRI are very similar to the ground-truth. However, there are different levels of noise in the targets in Figure 10c,f. Thus, the segmentation results of the proposed FSEFTISRI algorithm are more advantageous. It should be noted that the EITMIS algorithm fails in most NDT images because it is not suitable for small target image segmentation.

The comparison results of performance indexes of each algorithm for NDT images are shown in Table 1. Table 1 indicates that the performance of the proposed FSEFTISRI algorithm is better than the comparison algorithms, which is basically consistent with the results of visual effect, indicating that the proposed FSEFTISRI has great applicability to the images in the NDT Database.

#### 4.2.2. Analysis of Experimental Results of BSDS

BSDS is a popular image benchmark. The early BSDS contains 300 images, so it is called BSDS300. Now BSDS has 500 images, so it is called BSDS500. The images in BSDS are basically natural images with the same size of  $321 \times 481$ , and there is often environmental noise during acquisition. This section will objectively discuss the segmentation performance of the proposed FSEFTISRI algorithm from two aspects: visual effect and quantitative assessment.

The visual effects of the proposed FSEFTISRI algorithm and the five comparison algorithms for image segmentation are shown in Figures 11–16. According to Figures 11–16, the proposed FSEFTISRI has a good segmentation effect on images from BSDS and can completely segment the target and background.

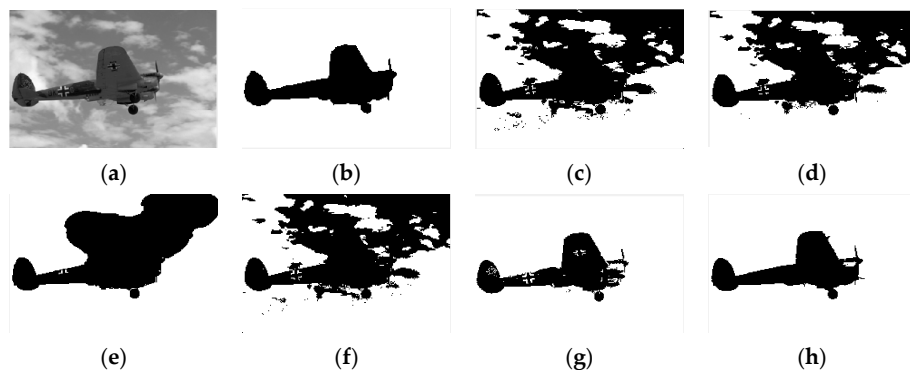


**Figure 11.** #3063 and its segmentations: (a) #3063, (b) ground-truth, (c) Otus, (d) MRCUT, (e) EITMIS, (f) NSWCC, (g) IT2FSWCC, (h) FSEFTISRI.

**Table 1.** Comparison of evaluation indexes of several algorithms in NDT images.

Image	Evaluation Indexes	Algorithms					
		Otus	MRCUT	EITMIS	NSWCC	IT2FSWCC	FSEFTISRI
#image1	ME	0.0665	0.4394	0.0181	0.0665	0.0392	0.0136
	FSIM	0.7430	0.4252	0.9587	0.7430	0.8365	0.9687
	PSNR	11.8046	3.5722	17.7079	11.8046	14.1568	19.3667
	SSIM	0.5654	0.0721	0.8817	0.5654	0.7463	0.8986
#image2	ME	0.5255	0.3381	0.0044	0.4943	0.0032	0.0008
	FSIM	0.2391	0.3021	—	0.2397	0.9686	0.9933
	PSNR	2.7941	4.7094	23.5946	3.0602	24.9415	30.8839
	SSIM	0.0024	0.0041	0.9508	0.0027	0.9542	0.9848
#image3	ME	0.5448	0.3681	0.0238	0.5132	0.0075	0.0015
	FSIM	0.3310	0.3358	—	0.3257	0.9753	0.9949
	PSNR	2.6378	4.3407	16.2351	2.8975	21.232	28.2217
	SSIM	0.0087	0.0173	0.9145	0.0088	0.9573	0.9891
#image6	ME	0.4466	0.4780	0.0652	0.4281	0.0438	0.0196
	FSIM	0.5899	0.5831	—	0.5976	0.8428	0.9139
	PSNR	3.5011	3.2054	11.8589	3.6844	13.5845	17.0671
	SSIM	0.1208	0.0943	0.731	0.127	0.7389	0.8162
#image13	ME	0.0218	0.4397	0.0588	0.0195	0.0218	0.0065
	FSIM	0.7311	0.2354	—	0.744	0.9466	0.9818
	PSNR	16.6133	3.5684	12.3031	17.0987	16.6133	21.8552
	SSIM	0.5573	0.0181	0.8555	0.5926	0.8771	0.9363
#image22	ME	0.0326	0.0678	0.8378	0.0326	0.0751	0.0256
	FSIM	0.9571	0.7785	—	0.9571	0.9136	0.9750
	PSNR	17.5937	12.5955	0.8353	17.5937	1.8914	20.8514
	SSIM	0.8511	0.6343	0.11	0.8511	0.7897	0.9053

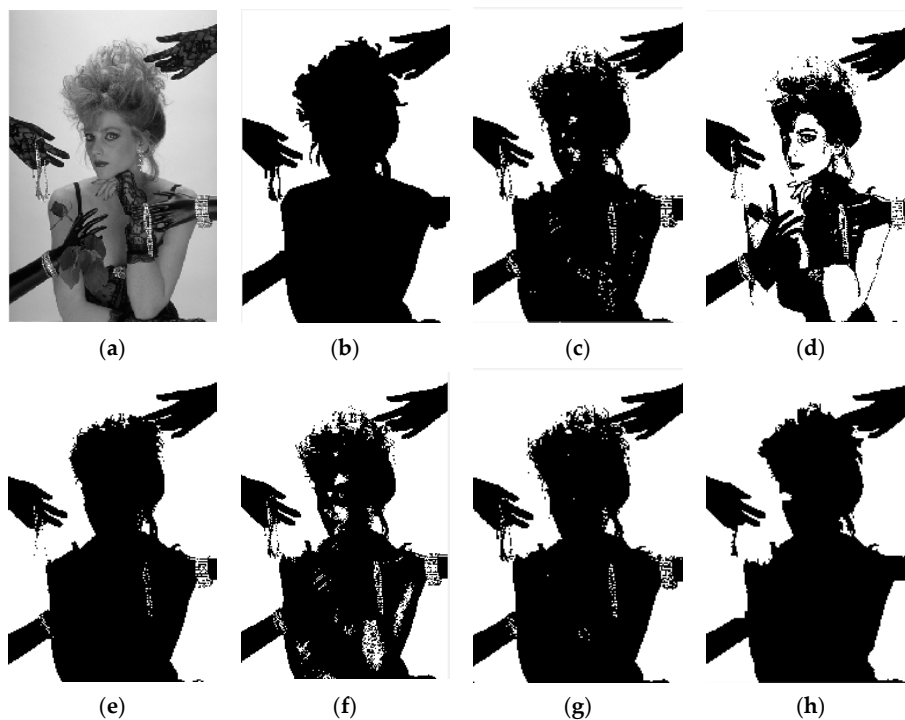


**Figure 12.** #198087 and its segmentations: (a) #198087, (b) ground-truth, (c) Otus, (d) MRCUT, (e) EITMIS, (f) NSWCC, (g) IT2FSWCC, (h) FSEFTISRI.

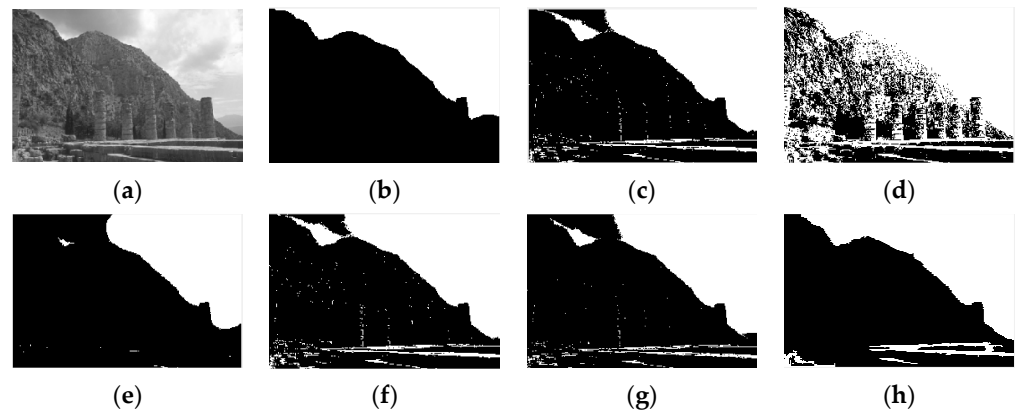


**Figure 13.** #227046 and its segmentations: (a) #227046, (b) ground-truth, (c) Otus, (d) MRCUT, (e) EITMIS, (f) NSWCC, (g) IT2FSWCC, (h) FSEFTISRI.

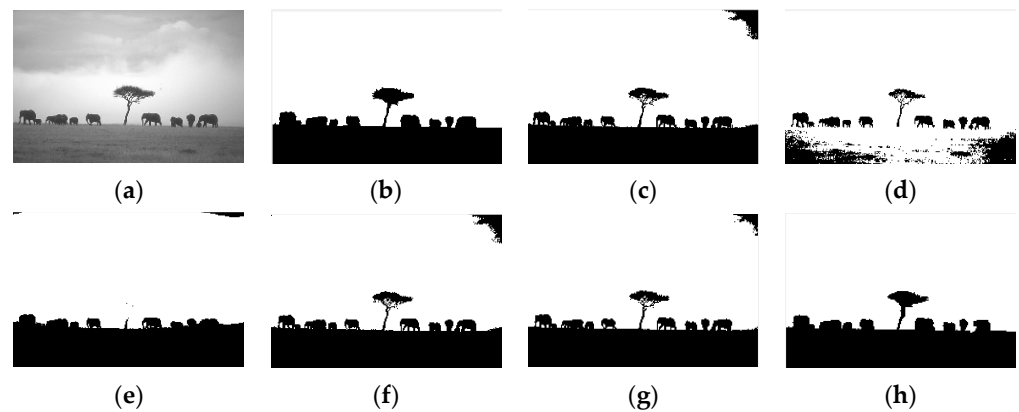


**Figure 14.** #253026 and its segmentations: (a) #253026, (b) ground-truth, (c) Otus, (d) MRCUT, (e) EITMIS, (f) NSWCC, (g) IT2FSWCC, (h) FSEFTISRI.

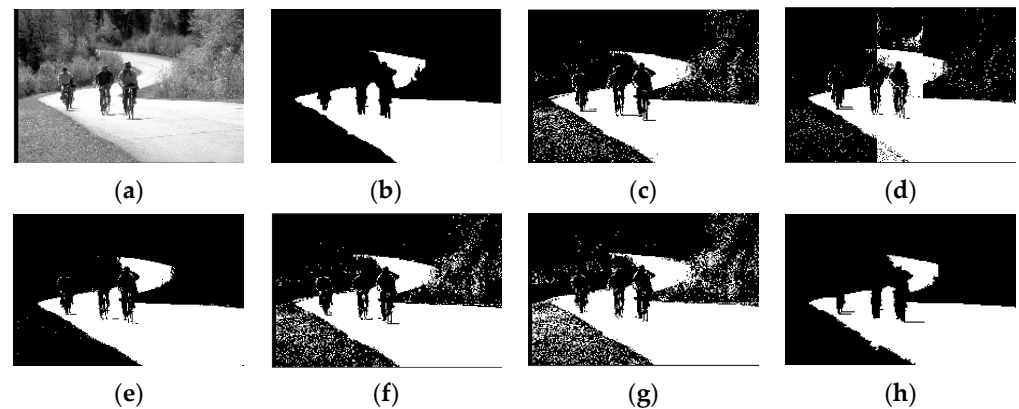


**Figure 15.** #344010 and its segmentations: (a) #344010, (b) ground-truth, (c) Otus, (d) MRCUT, (e) EITMIS, (f) NSWCC, (g) IT2FSWCC, (h) FSEFTISRI.

In Figure 11, the Otus, MRCUT, EITMIS and NSWCC algorithms cannot separate the cloud from the aircraft, while the IT2FSWCC algorithm extracts the target, but separates the “+” flag on the fuselage, making the target incomplete. The segmentation effect of the proposed FSEFTISRI is more ideal and closer to the standard segmentation. For the other five images, compared with the five comparison algorithms, the segmentation results of the proposed FSEFTISRI are relatively outstanding, and the target contains less noise.

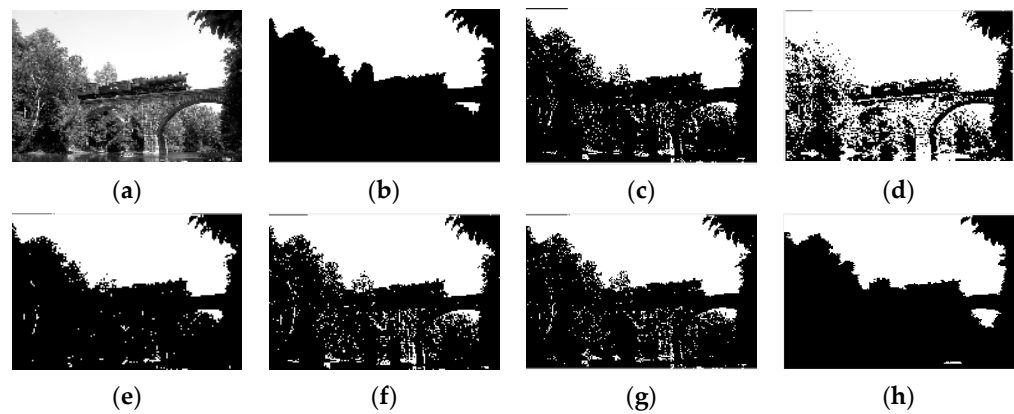


**Figure 16.** #351093 and its segmentations: (a) #351093, (b) ground-truth, (c) Otus, (d) MRCUT, (e) EITMIS, (f) NSWCC, (g) IT2FSWCC, (h) FSEFTISRI.

For images from BSDS, the EITMIS algorithm can obtain a relatively ideal effect, and there is no large number of failures like those in the NDT database, and the segmentation effect of Figure 15 is second only to that of the proposed FSEFTISRI algorithm.

For the six test images selected from BSDS, Table 2 lists the quantitative indexes of the segmentation results of each algorithm. From Table 2, the performance indexes of the proposed FSEFTISRI algorithm are mostly better than those of the comparison algorithms. Only in image #227046 are FSIM and SSIM slightly fewer than in the EITMIS algorithm. However, in light of the perspective of visual effect, the EITMIS algorithm divides the mountains into the same category as the sky in the upper left corner, which is visually different from the ground-truth. The comparison information in Table 2 indicates that the proposed FSEFTISRI can segment test images accurately without producing large amounts of distortion.

**Table 2.** Comparison of evaluation indexes of several algorithms in BSDS.

Image	Evaluation Indexes	Algorithms					
		Otus	MRCUT	EITMIS	NSWCC	IT2FSWCC	FSEFTISRI
#3063	ME	0.2923	0.2777	0.2115	0.2851	0.0194	0.0109
	FSIM	0.9241	0.9413	0.9638	0.9317	0.9931	0.9973
	PSNR	53.4723	53.6944	54.8771	58.5813	65.2519	67.7694
	SSIM	0.5685	0.6106	0.7404	0.5850	0.9230	0.9568
#198087	ME	0.0598	0.2092	0.0549	0.0997	0.0446	0.0441
	FSIM	0.9540	0.9330	0.9749	0.9494	0.9725	0.9889
	PSNR	60.3611	54.9245	60.7380	59.1137	61.6376	61.6897
	SSIM	0.7905	0.6110	0.8442	0.7513	0.8424	0.8704
#227046	ME	0.0639	0.3227	0.0521	0.0623	0.0670	0.0467
	FSIM	0.9152	0.8426	0.9824	0.9110	0.9403	0.9748
	PSNR	60.0763	53.0431	60.9653	60.1856	59.8675	61.4355
	SSIM	0.7620	0.3586	0.9162	0.7530	0.8024	0.8899
#253036	ME	0.0227	0.1820	0.0276	0.0210	0.0159	0.0060
	FSIM	0.9930	0.9731	0.9888	0.9938	0.9960	0.9986
	PSNR	64.5655	55.5306	63.7161	64.9065	66.1239	70.3653
	SSIM	0.9322	0.7252	0.9377	0.9338	0.9396	0.9699
#344010	ME	0.0604	0.0538	0.0179	0.0636	0.0998	0.0170
	FSIM	0.8948	0.9046	0.9900	0.8930	0.8716	0.9947
	PSNR	60.3199	60.8202	65.6098	60.0988	58.1393	65.8244
	SSIM	0.6205	0.6865	0.9003	0.6160	0.5691	0.9240
#351093	ME	0.0565	0.2712	0.0303	0.0624	0.0492	0.0264
	FSIM	0.8918	0.8379	0.9434	0.8818	0.8996	0.9932
	PSNR	60.6067	53.7984	63.3158	60.1788	61.2109	63.9203
	SSIM	0.6294	0.38831	0.7986	0.6084	0.6525	0.9154

### 4.2.3. Overall Analysis of Algorithm Performance Index

Due to there being 25 images in the NDT database and 500 images in the BSDS database, in order to evaluate the stability of the proposed FSEFTISRI, this section selects 50 images in BSDS and 10 images in the NDT for the experiment. The mean and variance of evaluation indexes of six algorithms are counted to verify the segmentation effect of the proposed FSEFTISRI, as listed in Tables 3 and 4.

**Table 3.** Mean value and variance of evaluation indexes of 6 algorithms in NDT images.

Index	Otus	MRCUT	EITMIS	NSWCC	IT2FSWCC	FSEFTISRI
ME	0.0118 ± 0.0110	0.2764 ± 0.0133	0.0794 ± 0.0099	0.1140 ± 0.0106	0.0951 ± 0.0069	0.0466 ± 0.0013
FSIM	0.9194 ± 0.0025	0.8911 ± 0.0026	0.9577 ± 0.0041	0.9178 ± 0.0024	0.9368 ± 0.0023	0.9811 ± 0.0002
PSNR	59.4565 ± 21.8622	54.3484 ± 7.7089	62.1613 ± 30.7761	59.4905 ± 18.9487	60.3545 ± 29.1880	63.1714 ± 21.5154
SSIM	0.6874 ± 0.0349	0.4917 ± 0.0300	0.8529 ± 0.0149	0.6866 ± 0.0341	0.7322 ± 0.0366	0.8949 ± 0.0041

**Table 4.** Mean value and variance of evaluation indexes of several algorithms in BSDS.

Index	Otus	MRCUT	EITMIS	NSWCC	IT2FSWCC	FSEFTISRI
ME	0.1986 ± 0.0484	0.2588 ± 0.0288	0.2977 ± 0.1252	0.1904 ± 0.0429	0.0499 ± 0.0024	0.0039 ± 0.0015
FSIM	0.6793 ± 0.0631	0.5543 ± 0.0481	0.9192 ± 0.0031	0.6808 ± 0.0635	0.8709 ± 0.0138	0.9257 ± 0.0049
PSNR	11.9394 ± 87.8907	7.1171 ± 13.9700	9.9438 ± 62.9851	12.5205 ± 112.3919	14.8075 ± 52.1845	18.9732 ± 49.7260
SSIM	0.4451 ± 0.1327	0.2622 ± 0.0785	0.5518 ± 0.1562	0.4496 ± 0.1336	0.7422 ± 0.0613	0.8245 ± 0.0277

According to Tables 3 and 4, the mean of the four indexes of the proposed FSEFTISRI algorithm are the best, and the variance is small. This shows that the segmentation results of the proposed FSEFTISRI algorithm have obvious advantages among the six algorithms, and are more stable.

In addition, the indexes of 50 images in BSDS are made into line charts to further demonstrate the segmentation effect of the proposed FSEFTISRI, as shown in Figures 17–20.

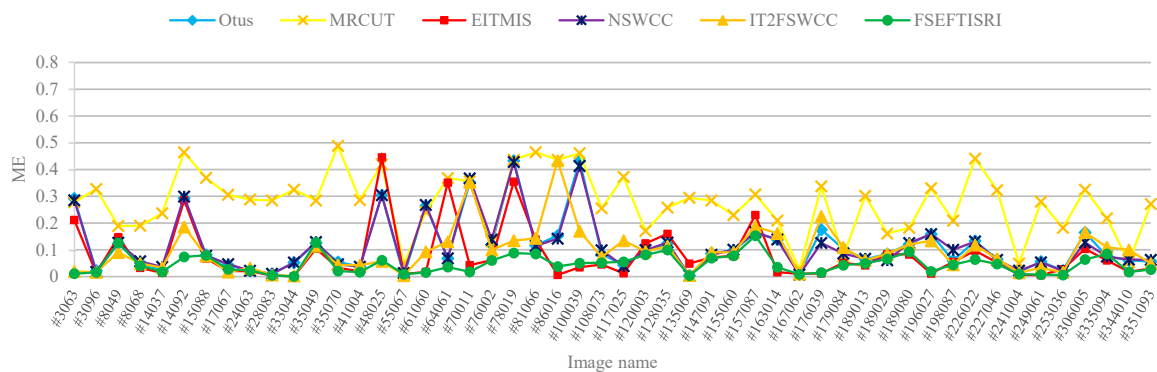


**Figure 17.** Comparison of ME of several algorithms.

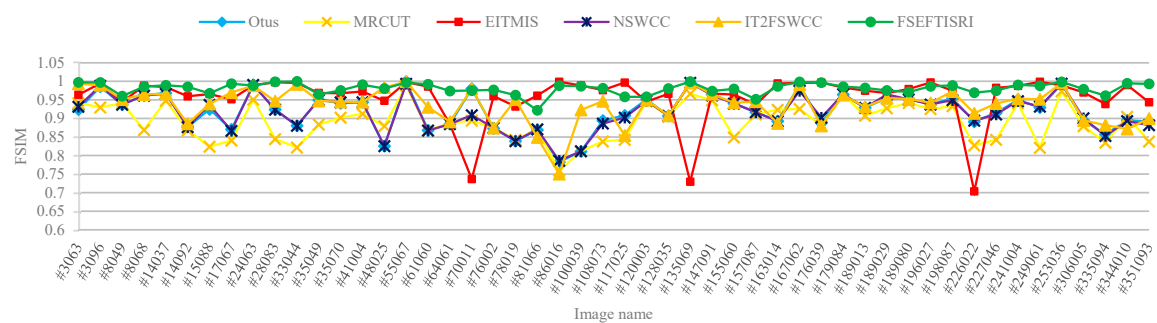


**Figure 18.** Comparison of FSIM of several algorithms.

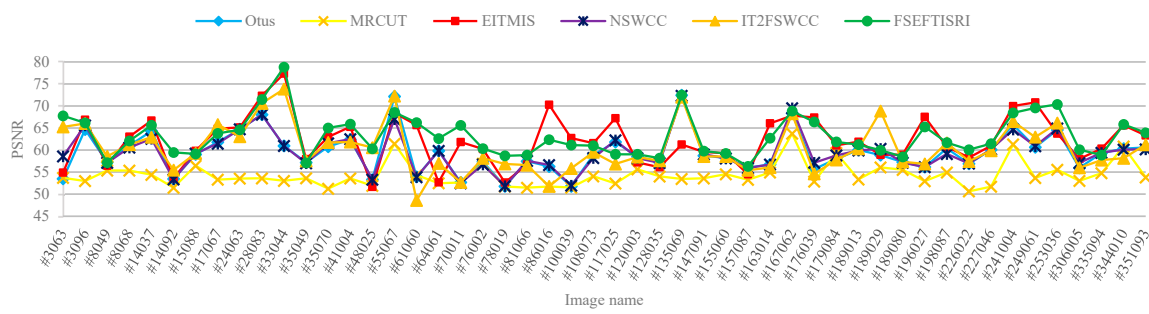


Figure 19. Comparison of PSNR of several algorithms.

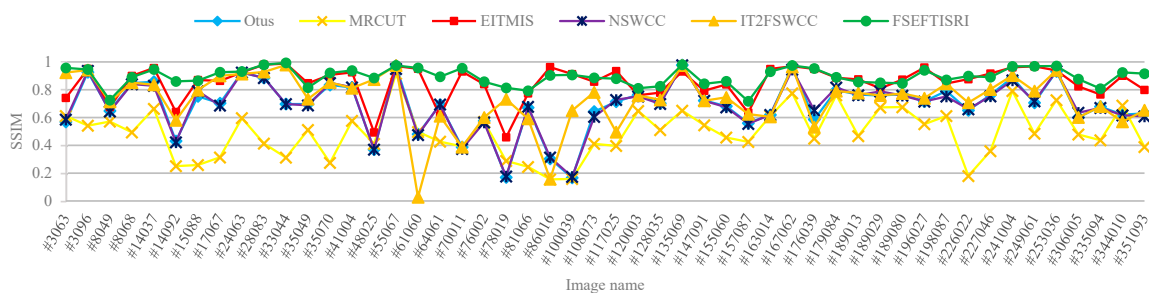


Figure 20. Comparison of SSIM of several algorithms.

According to the comparison of the line chart graph in Figure 17, the ME of the proposed FSEFTISRI is maintained below 0.16, and the line chart is at the lowest, indicating that the proposed FSEFTISRI can obtain greater accuracy. In the other three indexes shown in Figures 18–20, the performance of the proposed FSEFTISRI is also basically maintained at the highest level. These line charts show that the proposed FSEFTISRI algorithm has high segmentation accuracy, a pleasant segmentation effect, and certain stability.

#### 4.2.4. Comparative Experiment of the Operation Efficiency

In order to directly reflect the superiority of the proposed FSEFTISRI algorithm in terms of operating efficiency, the CPU consumption of the proposed FSEFTISRI algorithm and the comparison algorithms under the same software and hardware conditions is calculated. Since images in the BSDS are the same size, this section counts the running time of each algorithm in 50 images in BSDS and calculates the average CPU running time, as shown in Figure 21. At the same time, in order to avoid contingency, the variance of the running time of these 50 images is also shown in Table 4.

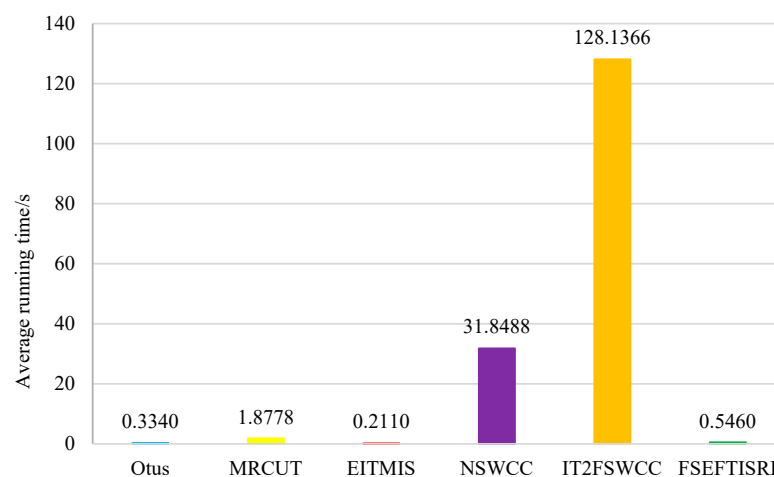


Figure 21. Comparison of the average running time of several algorithms.

Figure 21 illustrates that the operating efficiency of the proposed FSEFTISRI is only inferior to Otus, because Otus only calculates the gray information of the image, has low complexity, and its segmentation accuracy is not high either. The proposed FSEFTISRI algorithm not only consumes less CPU time, but can also obtain ideal segmentation results. The proposed FSEFTISRI greatly improves the running efficiency by using super-pixel technology, and the CPU time of the proposed FSEFTISRI is much less than it is for IT2FSWCC, which is consistent with the analysis result of computational complexity in Section 3.5.

Table 5 shows the variance of the running time of several algorithms on 50 images from BSDS. The variance of the proposed FSEFTISRI algorithm is only 0.0011. Combined with the running time of Figure 21, it can be concluded that the running time of the proposed FSEFTISRI algorithm is short.

**Table 5.** Variance of running time of several algorithms.

Algorithms	Otus	MRCUT	EITMIS	NSWCC	IT2FSWCC	FSEFTISRI
Variance of running time	0.0208	0.2843	0.3365	25.6121	3017.7348	0.0011

## 5. Conclusions

To solve the problems that IT2FSWCC algorithm has in terms of low computational efficiency and parameters that cannot be selected adaptively, this paper proposes a fast single-parameter energy function thresholding for image segmentation based on region information. In this paper, the original energy function is improved by SLIC, and the objective function of the proposed FSEFTISRI algorithm is constructed, which improves the operation efficiency of the proposed FSEFTISRI algorithm. The idea of extended neighborhood is adopted to extract the spatial features of super-pixels, avoiding the manual selection of spatial parameters. The theory of quasi-uncertainty is used to promote the penalty terms to play a role in the energy function and to select the penalty parameters adaptively, reducing the impact of the manual selection of parameters on the performance of the algorithm. The experimental results show that the proposed FSEFTISRI can obtain ideal segmentation results for NDT images and natural images in BSDS. Compared with the comparison algorithms, the proposed FSEFTISRI has higher efficiency under the condition of ensuring segmentation accuracy.

The proposed FSEFTISRI uses SLIC to divide the image into super-pixels. However, SLIC needs to preset the number of super-pixels, which limits the automaticity of the proposed FSEFTISRI to the image to a certain extent. Future studies will focus on the adaptive selection of the number of super-pixels so as to improve the adaptability of the algorithm to different types of images and improve the segmentation performance.

**Author Contributions:** Conceptualization, R.L. and D.F.; methodology, R.L. and D.F.; software, D.F.; validation, D.F.; writing—original draft preparation, D.F.; writing—review and editing, R.L. And D.F.; funding acquisition, F.Z., J.F. and H.Y. All authors have read and agreed to the published version of the manuscript.

**Funding:** This research is funded by the National Natural Science Foundation of China under grant number 62071379, by the National Natural Science Foundation of China under grant number 62071378, and by the National Natural Science Foundation of China under Grant No. 62106196, and by the New Star Team of Xi'an University of Posts & Telecommunications of China under Grant xyt2016-01.

**Data Availability Statement:** Publicly available datasets were analyzed in this study. This data can be found here: [<http://mehmetsezgin.net>. and <https://www.eecs.berkeley.edu/Res./Projects/CS/vision/bsds/>].

**Conflicts of Interest:** The authors declare that they have no known competing financial interests or personal relationships that could have appeared to influence the work reported in this paper.

## Abbreviations

The following abbreviations are used in this manuscript:

BSDS	Berkeley Segmentation Datasets and Benchmarks
CPU	central processing unit
EITMIS	An efficient iterative thresholding method for image segmentation
FSEFTISRI	fast single-parameter energy function thresholding for image segmentation based on region information fusion
FSIM	feature similarity
IT2FS	interval type-2 fuzzy set
IT2FSWCC	interval type-2 fuzzy set and theory of weak continuity constraints
ME	mis-classification error
MRCUT	multi-scale region and class uncertainty theory
NDT	Non-destructive testing
NSWCC	neutrosophic set and weak continuity constraints
PSNR	peak signal-to-noise ratio
SLIC	simple linear iterative clustering
SSIM	structural similarity index measure

## References

- Li, A.; Li, Y.; Wang, T.; Niu, W. Medical image segmentation based on maximum entropy multi-threshold segmentation optimized by improved cuckoo search algorithm. In Proceedings of the 2015 8th International Congress on Image and Signal Processing (CISP), Shenyang, China, 14–16 October 2015; IEEE: Shenyang, China; pp. 470–475. [\[CrossRef\]](#)
- Sehgal, S.; Kumar, S.; Bindu, M.H. Remotely sensed image thresholding using OTSU & differential evolution approach. In Proceedings of the International Conference on Cloud Computing, Noida, India, 12–13 January 2017; IEEE: Noida, India; pp. 138–142. [\[CrossRef\]](#)
- Medhi, J.P.; Nirmala, S.R.; Choudhury, S.; Dandapat, S. Improved detection and analysis of Macular Edema using modified guided image filtering with modified level set spatial fuzzy clustering on Optical Coherence Tomography images. *Biomed. Signal Process. Control* **2023**, *79*, 104149. [\[CrossRef\]](#)
- Bigand, A.; Colot, O. Membership function construction for interval-valued fuzzy sets with application to Gaussian noise reduction. *Fuzzy Sets Syst.* **2016**, *286*, 66–85. [\[CrossRef\]](#)
- Dhar, S.; Kundu, M.K. A novel method for image thresholding using interval type-2 fuzzy set and Bat algorithm. *Appl. Soft Comput.* **2018**, *63*, 154–166. [\[CrossRef\]](#)
- Wang, Y.; Chen, L.; Zhou, J.; Li, T.; Chen, C.P. Interval type-2 outlier-robust picture fuzzy clustering and its application in medical image segmentation. *Appl. Soft Comput.* **2022**, *122*, 108891. [\[CrossRef\]](#)
- Saha, P.; Udupa, J. Optimum image thresholding via class uncertainty and region homogeneity. *IEEE Trans. Pattern Anal. Mach. Intell.* **2001**, *23*, 689–706. [\[CrossRef\]](#)
- Wang, Y.; Liang, G.; Huang, S.; Wang, C.; Wu, X.; Feng, Y. A robust optimum thresholding method based on local intensity mapping and class uncertainty theory. In Proceedings of the 2017 IEEE International Conference on Information and Automation (ICIA), Macao, China, 18–20 July 2017; IEEE: Macao, China; pp. 317–322. [\[CrossRef\]](#)
- Zhou, L.; Jiang, Y.; Liang, G.; Wu, X.; Zhu, J.; Xiang, H. An Image Segmentation Method by Multi-scale Local Thresholding Based on Class Uncertainty Theory. In Proceedings of the 2019 IEEE International Conference on Robotics and Biomimetics (ROBIO), Dali, China, 6–8 December 2019; IEEE: Dali, China; pp. 2938–2944. [\[CrossRef\]](#)
- Liang, G.; Su, Y.; Chen, F.; Long, H.; Song, Z.; Gan, Y. Wind Power Curve Data Cleaning by Image Thresholding Based on Class Uncertainty and Shape Dissimilarity. *IEEE Trans. Sustain. Energy* **2020**, *12*, 1383–1393. [\[CrossRef\]](#)
- Dhar, S.; Kundu, M.K. Multi-class Image Segmentation Using Theory of Weak String Energy and Fuzzy Set. In *Intelligence Enabled Research in Advances in Intelligent System & Computing Book (AISC)*, 1st ed.; Springer: Singapore, 2020; Chapter 5; pp. 30–40. [\[CrossRef\]](#)
- Dhar, S.; Kundu, M.K. Interval Type-2 Fuzzy Set and Theory of Weak Continuity Constraints for Accurate Multiclass Image Segmentation. *IEEE Trans. Fuzzy Syst.* **2019**, *28*, 2151–2163. [\[CrossRef\]](#)
- Dhar, S.; Kundu, M.K. Accurate multi-class image segmentation using weak continuity constraints and neutrosophic set. *Appl. Soft Comput.* **2021**, *112*, 107759. [\[CrossRef\]](#)
- Achanta, R.; Shaji, A.; Smith, K.; Lucchi, A.; Fua, P.; Süsstrunk, S. SLIC Superpixels Compared to State-of-the-Art Superpixel Methods. *IEEE Trans. Pattern Anal. Mach. Intell.* **2012**, *34*, 2274–2282. [\[CrossRef\]](#)
- Lei, T.; Jia, X.; Zhang, Y.; Liu, S.; Meng, H.; Nandi, A.K. Superpixel-Based Fast Fuzzy C-Means Clustering for Color Image Segmentation. *IEEE Trans. Fuzzy Syst.* **2018**, *27*, 1753–1766. [\[CrossRef\]](#)
- Di, S.; Liao, M.; Zhao, Y.; Li, Y.; Zeng, Y. Image superpixel segmentation based on hierarchical multi-level LI-SLIC. *Opt. Laser Technol.* **2020**, *135*, 106703. [\[CrossRef\]](#)

17. He, F.; Mahmud, M.P.; Kouzani, A.Z.; Anwar, A.; Jiang, F.; Ling, S.H. An Improved SLIC Algorithm for Segmentation of Microscopic Cell Images. *Biomed. Signal Process. Control* **2021**, *73*, 103464. [[CrossRef](#)]
18. Zhang, Y.; Zhang, Y.; Fan, L.; Wang, N. Fast and accurate superpixel segmentation algorithm with a guidance image. *Image Vis. Comput.* **2022**, *129*, 104596. [[CrossRef](#)]
19. Mendel, J.M.; John, R.I.; Liu, F. Interval Type-2 Fuzzy Logic Systems Made Simple. *IEEE Trans. Fuzzy Syst.* **2006**, *14*, 808–821. [[CrossRef](#)]
20. Arbelaez, P.; Maire, M.; Fowlkes, C.; Malik, J. Contour Detection and Hierarchical Image Segmentation. *IEEE Trans. Pattern Anal. Mach. Intell.* **2011**, *33*, 898–916. [[CrossRef](#)] [[PubMed](#)]
21. Otsu, N. A threshold selection method from gray-level histograms. *IEEE Trans. Syst. Man Cybern.* **1979**, *9*, 62–66. [[CrossRef](#)]
22. Wang, D.; Li, H.; Wei, X.; Wang, X.-P. An efficient iterative thresholding method for image segmentation. *J. Comput. Phys.* **2017**, *350*, 657–667. [[CrossRef](#)]
23. Zou, Y.; Liu, H.; Zhang, Q. Image bilevel thresholding based on stable transition region set. *Digit. Signal Process.* **2012**, *23*, 126–141. [[CrossRef](#)]
24. Zhang, L.; Zhang, L.; Mou, X.; Zhang, D. FSIM: A Feature Similarity Index for Image Quality Assessment. *IEEE Trans. Image Process.* **2011**, *20*, 2378–2386. [[CrossRef](#)]
25. Lei, B.; Fan, J. Image thresholding segmentation method based on minimum square rough entropy. *Appl. Soft Comput. J.* **2019**, *84*, 105687. [[CrossRef](#)]
26. Kumar, A.; Kumar, A.; Vishwakarma, A.; Lee, H.N. An improved segmentation technique for multilevel thresholding of crop image using cuckoo search algorithm based on recursive minimum cross entropy. *IET Signal Process.* **2022**, *16*, 630–649. [[CrossRef](#)]
27. Sezgin, M.; Sankur, B.L. Survey over image thresholding techniques and quantitative performance evaluation. *J. Electron. Imaging* **2004**, *13*, 146–168. [[CrossRef](#)]

**Disclaimer/Publisher’s Note:** The statements, opinions and data contained in all publications are solely those of the individual author(s) and contributor(s) and not of MDPI and/or the editor(s). MDPI and/or the editor(s) disclaim responsibility for any injury to people or property resulting from any ideas, methods, instructions or products referred to in the content.